

Differentiable Machine Learning-Based Modeling for Directly-Modulated Lasers

Sergio Hernandez Fernandez, *Student Member, IEEE*, Ognjen Jovanovic *Member, IEEE*,
Christophe Peucheret *Member, IEEE*, Francesco Da Ros *Senior Member, IEEE*, Darko Zibar

Abstract—End-to-end learning has become a popular method for joint transmitter and receiver optimization in optical communication systems. Such approach may require a differentiable channel model, thus hindering the optimization of links based on directly modulated lasers (DMLs). This is due to the DML behavior in the large-signal regime, for which no analytical solution is available. In this paper, this problem is addressed by developing and comparing differentiable machine learning-based surrogate models. The models are quantitatively assessed in terms of root mean square error and training/testing time. Once the models are trained, the surrogates are then tested in a numerical equalization setup, resembling a practical end-to-end scenario. Based on the numerical investigation conducted, the convolutional attention transformer is shown to outperform the other models considered.

Index Terms—Optical communication, machine learning, directly modulated laser, transformer, modeling

I. INTRODUCTION

Directly-modulated lasers (DMLs) play a crucial role as part of intensity-modulation and direct-detection (IM/DD) systems in short-reach communication links. Due to their inherent simplicity, DMLs have the potential to achieve efficiency gains in both power consumption and cost-effectiveness compared to alternative transmitter technologies [1]. However, their modulation bandwidth (around 30 GHz at 25 °C) limits the symbol rate of commercial DMLs to the 50 Gbaud range, making them a less compelling option as Ethernet throughput requirements increase [2]. Apart from the ever-present phase and intensity noise, effects such as waveform distortion or frequency chirping dominate when pushing their modulation rate, hindering their potential in terms of transmission distance and data throughput. One can benefit from an increased modulation bandwidth by driving the laser with higher current values, at the cost of a lower extinction ratio and degraded sensitivity. Finding an optimal balance between signal degradation mechanisms is therefore a complex task. This has led to the investigation of different mitigation techniques to increase the symbol rate while maintaining a sufficient signal quality.

Equalization (EQ) and pre-distortion have been broadly used in this context, as they force the received signal to resemble the original unaltered waveform. Nevertheless, previous equalization solutions have relied on the separate optimization of the transmitter and receiver, disregarding the potential gains obtained through their simultaneous optimization [3],

[4]. To achieve further data throughput improvements, joint optimization of the transmitter and receiver using end-to-end (E2E) learning has gained traction as an optimization approach for optical communication systems, pushing their performance closer to their theoretical capacity [5], [6].

The conventional approach to gradient-based optimization in E2E learning is based on a differentiable channel model [5]. The DML small-signal response can be easily approximated by differentiable methods, at the cost of constraining the peak-to-peak amplitude of the modulated signal to impractically low levels in a realistic scenario. The more suitable large-signal dynamics are however governed by nonlinear differential rate equations, for which no analytical solution can be obtained [7]. This limitation poses challenges in achieving a differentiable channel. Although ordinary differential equation (ODE) solvers and optimization approaches (reinforcement learning, gradient-free) have been proposed as gradient estimators, they often require considerable computational overhead [8]. To enable E2E learning and facilitate the estimation of gradients within the communication system, a locally accurate DML model is required [9].

This letter builds upon our work in [10] showcasing the application of data-driven optimization techniques to derive differentiable DML models. The model performance analysis is based on four different data-driven models, namely time-delay neural networks (TDNN), Volterra filters, long-short term memory (LSTM) and convolutional attention transformers (CATs). In this work we integrate each model into a new system optimization setup and conduct a comparative analysis of the generated signals with the laser rate equation output. The objective is to evaluate the models' gradient estimation performance from a more contextualized perspective as part of a larger optimization system, instead of assessing them as mere function estimators. A quantitative comparison between the models is conducted in terms of normalized root mean square error (NRMSE) and train/test time, while providing a visual qualitative comparison through the use of eye diagrams.

Comparing the different architectures, the results show that the CAT model is able to achieve improved NRMSE performance in training and testing throughout the analyzed symbol rates while maintaining a GPU processing time comparable to its alternatives. CATs are therefore expected to offer an efficient solution for optimizing DML-based communication systems where the direct use of ODE solvers would be impractical.

This work was financially supported by the ERC-CoG FRECOM project (no. 771878) and the Villum YIP OPTIC-AI project (no. 29334).

Manuscript received April 19, 2021; revised August 16, 2021.

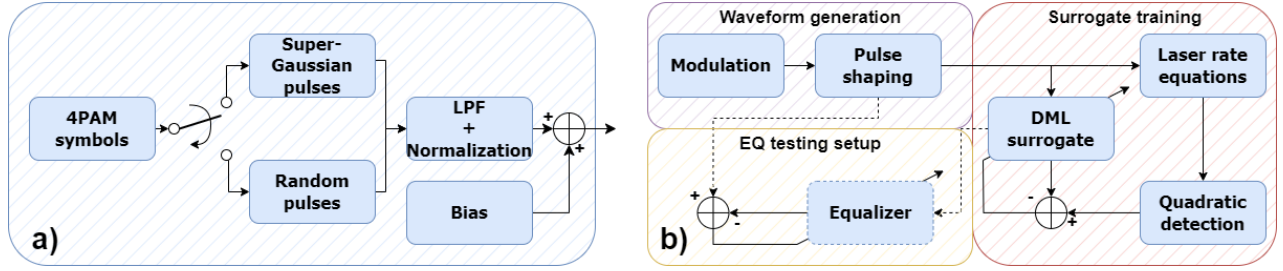


Fig. 1. Block diagrams of a) data acquisition and b) model setup

II. NUMERICAL SETUP

A. Data-Driven Modeling

Any data-driven model design presents two fundamental choices: the model structure to be used and the data features fed into it. Domain knowledge is key in both decisions, as the characteristics of the task to be performed may better suit some architectures over others. Alternatively to more established techniques in laser modeling, like circuit-level models [6], we propose the utilization of CATs [11]. CATs employ convolutions to model the dependencies within temporal sequences. This approach offers several advantages: (i) it restricts the utilization of past sequence samples in prediction, (ii) it captures waveform patterns rather than individual sample relations, and (iii) it has strong awareness of the order of the samples within the sequence. Although recurrent architectures are also based on temporal context, they need to calculate previous states sequentially in order to infer future samples. CATs break this bottleneck by processing the full time sequences at once, making better use of parallelization hardware and memory resources [11].

To maximize the accuracy of the data-driven model across various scenarios, the input data must encompass a wide range of waveforms and amplitudes, providing deep understanding of the laser's dynamic behaviour. Ideally, the pulse shaping block generating the data should use few input parameters while yielding a large amount of different output waveforms to avoid overfitting. This is addressed, as shown in Fig. 1a, by alternating between two types of pulse shapes: super-Gaussian pulses and random pulses. The random pulses are sampled as vectors from a folded normal distribution $\mathcal{N}(0.5, 1)$. The parameters for the super-Gaussian pulses, namely the temporal full width $e^{-0.5}$, T_0 and the order n are sampled from a folded $\mathcal{N}(0.25T_{\text{sym}}, T_{\text{sym}})$ and uniform $\mathcal{U}(1, 6)$ distributions, respectively. T_{sym} is the symbol period, reciprocal of the symbol rate. The amplitude of the pulses is modulated according to equiprobable pulse-amplitude modulation (4PAM) symbols. Subsequently, the pulses undergo min-max normalization and low-pass filtering (LPF) to prevent out-of-band leakage. The pulse shaping is randomized again every 8 symbols (with 32 samples per symbol) until completing a 1024-sample sequence of mixed pulse shapes. The training data set comprises 2^{13} sequences, totaling 2^{23} samples, while the validation set consists of 2^{17} samples. The target training data is obtained based on numerical simulations obtained from the general laser rate equations [12], using the aforementioned

TABLE I
MODEL HYPERPARAMETERS USED

	CAT	TDNN	LSTM
Number of hidden nodes	128	2048	64
Number of hidden layers	2	1	2
Activation function	ReLU	ReLU	ReLU
Number of MLP sublayers	2	2	-
Convolutional window length	9	31	-
Embedd. size	128	-	-
Number of attention heads	8	-	-

stochastic waveforms as input. The symbol rate of the driving signal is varied to introduce different levels of distortion, obtaining a distinct model for every symbol rate investigated. To solve the laser rate equations, a fifth-order Runge-Kutta (RK4,5) solver is utilized. As shown in Fig. 1b, the solution obtained from the solver serves as the ground truth for the surrogate models, establishing the relationship between the input modulation current (generated waveform) and the laser output after quadratic detection (optical power).

The proposed CAT model adopts a decoder-only structure, consisting of three main blocks: learned positional embeddings (LPEs), convolutional attention sublayers, and 2-layer multilayer perceptrons (MLP) with ReLU hidden activation. A linear layer is employed to reduce the dimensionality of the hidden features. For comparison purposes, three additional models were investigated: a second-order Volterra filter with 16-sample memory, a TDNN, and an LSTM. The specific values for each network hyperparameter are summarized in Table I.

B. Equalization setup

To demonstrate the proof-of-concept, all the trained surrogate models were evaluated within a numerical back-to-back transmission setup with a receiver equalizer. Thus, their potential to achieve link gains in a real optimization environment can be showcased. A simple FIR-based equalizer trained on NRMSE was selected as testing scenario, as its simplicity allows to focus on the accuracy of the DML model. It is important to note that the optimality of the equalizer structure for this task is not a primary concern within the present scope, as the focus lies on the predictive potential of the surrogate models. The equalization task is performed on a per-sample basis, using square-pulse-shaped 4PAM symbols. It should be emphasized that none of the surrogate models was trained specifically on pure square waveforms, ensuring a fair assessment of their inference capabilities. As depicted

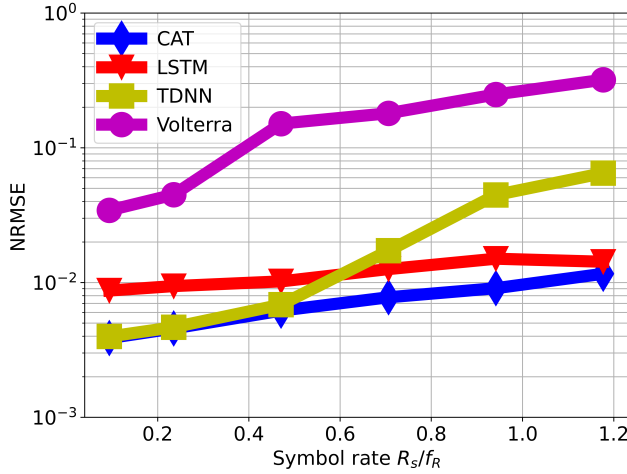


Fig. 2. NRMSE scores of the studied models

in Fig. 1b, the loss is calculated by calculating the NRMSE between the low-pass-filtered waveforms at the input of the DML and the signal at the output of the equalizer. Since the studied surrogates cannot perfectly replicate the laser rate equations, the learned equalizer coefficients are also tested on the output waveforms from the ODE solver to gain insight into the extent of metric distortion induced by the models. The comparison between the losses obtained from the surrogate models and the rate equation serves as the primary benchmark, as it reflects the generalization capabilities of each model in handling a previously unseen scenario.

III. NUMERICAL RESULTS

A. Surrogate models

The numerical simulations performed can be divided into surrogate and equalizer optimization. The DML response exhibits spectral characteristics that cause waveform distortion to increase as the symbol rate R_s increases, especially beyond the relaxation frequency f_R . The high-rate region close to f_R is therefore of particular interest. Within the surrogate training, we evaluated models across six distinct symbol rates, spanning the range $0.1f_R$ to $1.2f_R$. In each instance, we used an Adam optimizer with recommended decay values ($\beta_1 = 0.9, \beta_2 = 0.999$), along with min-max normalized mean square error (NMSE) as loss metric, later converted into its squared root form, NRMSE, for unit matching purposes. As a proof of concept, laser phase and intensity noise were not considered for simplicity. Each surrogate model was trained for 400 epochs, selecting the one achieving the lowest test loss. The optimal hyperparameters for each model were obtained through grid search. The selected models were then utilized for the equalization task, so their potential as part of a link optimization setup could be verified.

The most straightforward validation in a supervised time series inference model is to compare its predictions with the desired sequences sample by sample. This approach is shown in Fig. 2, where the NRMSE value is plotted as a function of the symbol rate. Over the symbol rates analyzed, most of the models deliver similar performance, although the CAT seems to deliver better performance than its peers and falls below

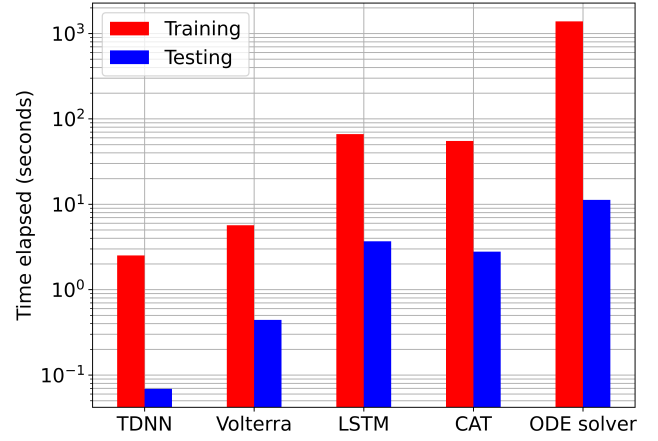


Fig. 3. Time elapsed (per epoch) by the presented models

the 10^{-2} mark. This is especially true for higher symbol rates, where only the LSTM is able to approach its performance. The Volterra-based model is the main outlier, with an error over 10% in the high rate region. Despite the substantial differences between the models, all the loss curves hint at the correlation between R_s and the waveform distortion introduced, showing that as the symbol duration becomes shorter, the output sequences are more difficult to match. The TDNN showcases this tendency, showing relatively good NRMSE figures at low R_s that worsen gradually as the symbol rate is increased. Further context is given in Fig. 3, where the average processing time for a train and test epoch on the utilized NVIDIA A100 GPU is compared. The ODE solver score shows the elapsed time for the generation of the target sequences. The figure pictures the importance of the model architecture in the inference speed of the networks: although the CAT has significantly more training parameters than the other surrogates, it operates at comparable times, even outperforming the LSTM. It is also clear that all of the proposed models add substantial time savings compared to the ODE solver. Another useful insight can be obtained by looking at Fig. 4, where the response of each model to a train of 4PAM Gaussian pulses is represented in the shape of eye diagrams. The output of the ODE solver to the same signal was added as a reference. Although all 4 models show reasonable convergence compared to the ODE case, there are some noticeable outliers. While the Volterra filter and the TDNN seem to oversimplify the DML dynamics compared to the ODE solver, the CAT is more sensitive to small changes in position and amplitude in samples. The former effect is probably due to the relatively low number of training parameters in the models, while the latter may be due to the one-to-many mapping in the positional encoding of the CAT. However, this drawback may be less relevant in real scenarios where noisy input data will affect the results of the output waveform to some extent. It must be noted that even if the eye diagrams give a good intuition of the behaviour of each model, they show the response to a very specific input, while the NRMSE scores yield a broader analysis throughout the different waveforms.

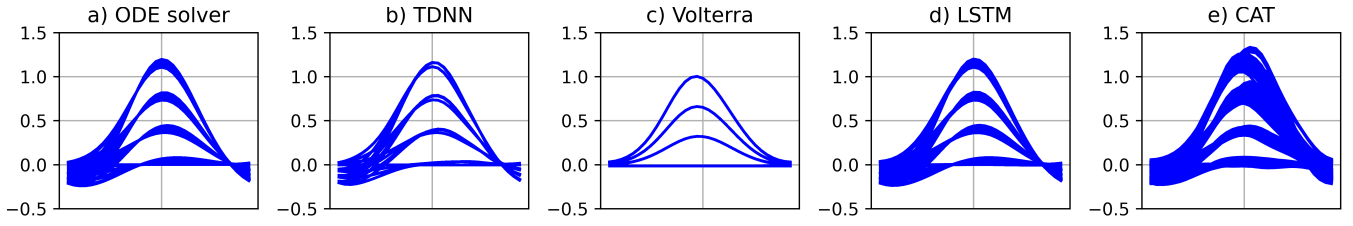


Fig. 4. Eye diagram of a 4PAM Gaussian pulse train at $R_s \approx f_R$ for a) ODE solver, b) TDNN, c) Volterra filter, d) LSTM and e) CAT.

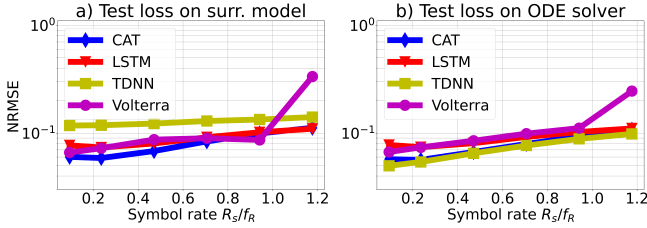


Fig. 5. Equalization NRMSE tested on a) surrogate models b) ODE solver

B. Equalizer optimization

Additional insights can be extracted from the equalization setup, where the MSE between the received and transmitted waveforms was obtained. The FIR equalizer is based on a trainable 31-tap filter, using random 4PAM transmitted symbols as a data source. In all cases, the symbol sequences utilized are identical for fair comparison. Fig. 5 establishes a comparison between the loss calculated based on the response of each of the models and the loss obtained when using the ODE solver as estimator of the laser response. It becomes apparent that, even though all of the surrogates yield similar overall performance, the difference between the two plots is significant in certain cases. While the LSTM and the CAT show almost identical curves in each case, the TDNN and Volterra MSE loss is significantly poorer when tested on themselves than on the ODE solver. This could be due to waveform artifacts (hinted in the eye diagrams) that distort the signal only when the testing is performed on the model, but make the equalizer more robust towards impairments during training. The Volterra filter seems to deliver a relatively solid response in the low-rate region, but it progressively degrades when approaching higher symbol rates. Even if the TDNN delivers the best ODE-based testing performance, its scores differ noticeably from the self-testing case, making it potentially unreliable as estimator of the DML response.

IV. CONCLUSIONS

This study has proposed a series of differentiable surrogate models for directly modulated laser links. In addition to the usual loss metrics, the models were tested in an equalizer-based optimization setup to showcase their prospects in a real setting. The analysis shows the complexity of choosing a model that resembles the laser response under every scenario and the variety of factors that must be taken into account. Throughout the metrics obtained, the convolutional attention transformer has shown high resilience to different waveforms

and symbol rates, while maintaining relatively low inference times thanks to its parallelization capabilities. Our results show the potential of data-driven models as faster substitutes for ODE solvers and derivative-free gradient approximators in the context of link optimization.

V. ACKNOWLEDGEMENTS

This work was financially supported by the ERC-CoG FRECOM project (no. 771878) and the Villum YIP OPTIC-AI project (no. 29334).

REFERENCES

- [1] J. Huang, C. Li, R. Lu, L. Li, and Z. Cao, "Beyond the 100 Gbaud Directly Modulated Laser for Short Reach Applications," *J. Semicond.*, vol. 42, no. 4, p. 041306, 2021.
- [2] S. Yamaoka, N.-P. P. Diamantopoulos, H. Nishi, T. Fujii, K. Takeda, T. Hiraki *et al.*, "Uncooled 100-Gbaud Directly Modulated Membrane Lasers on SiC Substrate," *J. Lightwave Technol.*, vol. 41, no. 11, pp. 3389–3396, 2023.
- [3] W.-H. Huang, H.-M. Nguyen, C.-W. Wang, M.-C. Chan, C.-C. Wei *et al.*, "Nonlinear Equalization Based on Artificial Neural Network in DML-Based OFDM Transmission Systems," *J. Lightwave Technol.*, vol. 39, no. 1, pp. 73–82, 2021.
- [4] K. Wang, M. Zhao, M. Kong, and J. Yu, "Demonstration of 4×100 Gbit/s PAM-4 Transmission Over 40 km in an IM/DD System Based on Narrow Band DMLs," *IEEE Photonics J.*, vol. 12, no. 3, pp. 1–8, 2020.
- [5] B. Karanov, M. Chagnon, V. Aref, D. Lavery, P. Bayvel, and L. Schmalen, "Concept and Experimental Demonstration of Optical IM/DD End-to-End System Optimization using a Generative Model," in *Optical Fiber Communications Conference and Exhibition (OFC)*, 2020, p. Th2A.48.
- [6] M. Srinivasan, J. Song, A. Grabowski, K. Szczerba, H. K. Iversen *et al.*, "End-to-End Learning for VCSEL-Based Optical Interconnects: State-of-the-Art, Challenges, and Opportunities," *J. Lightwave Technol.*, vol. 41, no. 11, pp. 3261–3277, 2023.
- [7] N. H. Zhu, Z. Shi, Z. K. Zhang, Y. M. Zhang, C. W. Zou *et al.*, "Directly Modulated Semiconductor Lasers," *IEEE J. Sel. Top. Quantum Electron.*, vol. 24, no. 1, p. 1500219, 2018.
- [8] M. P. Yankov, O. Jovanovic, D. Zibar, and F. D. Ros, "Recent Advances in Constellation Optimization for Fiber-Optic Channels," in *European Conference on Optical Communication (ECOC)*, 2022, p. Mo3D.4.
- [9] D. Wang, Z. Zhang, M. Zhang, M. Fu, J. Li *et al.*, "The Role of Digital Twin in Optical Communication: Fault Management, Hardware Configuration, and Transmission Simulation," *IEEE Commun. Mag.*, vol. 59, no. 1, pp. 133–139, 2021.
- [10] S. Hernandez, C. Peucheret, O. Jovanovic, F. D. Ros, and D. Zibar, "Data-Driven Modeling of Directly-Modulated Lasers," in *European Conference on Optical Communication (ECOC)*, 2023, p. M.A.3.3.
- [11] S. Li, X. Jin, Y. Xuan, X. Zhou, W. Chen *et al.*, "Enhancing the Locality and Breaking the Memory Bottleneck of Transformer on Time Series Forecasting," *Adv. Neural Inf. Process.*, vol. 32, p. 471, 2019.
- [12] L. A. Coldren, S. W. Corzine, and M. L. Mashanovitch, *Diode Lasers and Photonic Integrated Circuits*. John Wiley & Sons, 2012.